Microscopic study of steady convective flow in periodic systems

David R. J. Monaghan and Gary P. Morriss
School of Physics, University of New South Wales, Sydney, New South Wales 2052, Australia
(Received 9 January 1997)

We derive a consistent microscopic formulation that connects macroscopic hydrodynamic quantities with the microscopic positions and velocities of the constituent atoms. Introducing a local fluid streaming velocity, which is applied microscopically to separate the thermal and streaming motion of each particle, we obtain the microscopic representations for the pressure tensor and heat flux vector. The formalism is applied to a particular two-dimensional flow pattern termed four-roller flow. Molecular-dynamics results obtained indicate that the conservation equations are consistent at the microscopic level for four-roller flow. Molecular-dynamics results for the effective transport coefficients, shear viscosity, thermal conductivity, and a cross coefficient ξ at particular values of the k vector are obtained by analyzing the constitutive equations separately. [S1063-651X(97)05607-9]

PACS number(s): 47.10.+g, 05.20.−y, 51.20.+d

I. INTRODUCTION

The hydrodynamical conservation equations [1] describe the redistribution of the conserved quantities, such as mass, momentum, and energy, within a fluid. In the hydrodynamic description the fundamental unit is the volume element that must be large compared to atomic length scales, but small enough such that bulk properties do not change within an element. In this description we can define the value of a conserved quantity, or its flux, at an arbitrary position $\mathbf{r}$ and time t. The velocity of a fluid element at a given point in time and space is called the local streaming velocity $\mathbf{u}(\mathbf{r},t)$. For steady flows, the streaming velocity at each point in space is independent of time. The conservation equations are closed by the constitutive equations, Newton's law of viscosity, and Fourier's law of heat conduction. The resulting Navier-Stokes equations are partial differential equations that need to be solved for a given set of boundary conditions. Here our aim is to connect the hydrodynamic and microscopic descriptions for a particular class of flow problems, but rather than obtaining the Navier-Stokes equation, we keep the exact conservation equations separate from the approximate constitutive equations and explore their properties independently.

In the macroscopic formulation, the fluid element is the fundamental unit. The major problem in connecting the macroscopic and microscopic descriptions is developing a physically meaningful definition of the streaming velocity; this is connected with the identification and separation of macroscopic and microscopic length scales. In the microscopic description we have the positions and velocities of all the atoms. This description contains much more information than the macroscopic description simply because so many more variables are involved. In the microscopic picture, a given set of initial conditions and the equations of motion with a particular interaction potential give the position and velocity of each atom at each point in time. Often the fluid is subject to an external field or boundary condition that induces a specific bulk flow pattern. This may be equivalent to a hydrodynamic boundary condition. Macroscopically, the local streaming velocity of each of the fluid elements determines the bulk flow pattern. Our intention in defining the local streaming velocity $\mathbf{u}(\mathbf{r},t)$ is to use it on the microscopic length scale to identify the streaming component of the laboratory velocity of each particle. This means that the observed laboratory velocity $\dot{\mathbf{r}}_i(t)$ of each atom has two components: a local streaming velocity at the position of the particle $\mathbf{u}(\mathbf{r}_i,t)$ and a random or thermal velocity $\mathbf{v}_i(t)$. Thus the laboratory velocity of particle i is $\dot{\mathbf{r}}_i(t)=\mathbf{v}_i(t)+\mathbf{u}(\mathbf{r}_i,t)$. To determine the streaming velocity $\mathbf{u}(\mathbf{r},t)$ some type of averaging is required, either implicit or explicit in time or space. The temperature arises naturally in the microscopic picture through the random or thermal component of the velocities $\mathbf{v}_i(t)$.

In the development of the microscopic approach we begin by considering the densities of the macroscopically conserved quantities, that is, the mass, momentum and energy, as introduced by Irving and Kirkwood [2]. In the original Irving-Kirkwood procedure the mass density was defined to be the ensemble average of an instantaneous mass density. Here we return to the concept of an instantaneous mass density defined for each ensemble member (or set of microscopic initial conditions). From a computational point of view it is often more natural to calculate the system properties from a single long system trajectory rather than to construct the ensemble average. Similarly, the momentum and energy densities can be defined at each instant along a phase-space trajectory. Substituting the microscopic representations for the densities of conserved quantities into the conservation equations gives microscopic representations for the pressure tensor and the heat flux vector, which can be used in molecular-dynamics experiments.

The numerical values of the transport coefficients contained in the constitutive equations are considered as input quantities in the macroscopic hydrodynamic treatment. Microscopic methods are required to determine the numerical values of the transport coefficients from the intrinsic properties of the fluid. Such methods include, for example, the Green-Kubo method [3] using equilibrium fluctuations or nonequilibrium methods [4,5] such as the SLLOD algorithm for shear viscosity [4] and those of Evans [6] and Gillan and Dixon [7] for thermal conductivity. The Green-Kubo meth-

ods can calculate transport coefficients at nonzero k vector, but usually the nonequilibrium methods yield only zero-k-vector transport coefficients. However, an advantage of the nonequilibrium methods is that they often model the real physical process and can therefore give information about the nonlinear behavior of a fluid.

One of the earliest nonequilibrium methods to calculate the shear viscosity was to use a sinusoidal transverse force (STF) to drive a streaming velocity of the same functional form [8]. Knowing the ratio of the amplitudes of the streaming velocity and the force, the shear viscosity can be calculated from the Navier-Stokes equation. This method calculates the k-vector-dependent shear viscosity that only approaches the Navier-Stokes viscosity in the limit as $k\rightarrow 0$. This method was later exploited by Evans [9] to explicitly calculate the k- vector-dependent shear viscosity and investigate its behavior as a function of both the k vector and the amplitude of the driving force. Of particular interest was the functional dependence of the viscosity upon the k vector and the implications of this for the convergence of Burnett expansions in hydrodynamics [10]. Recently, calculations have been performed using the STF method [11] and a different heat flux mode discovered. This mode is a heat flux vector contribution proportional to the gradient of the square of the strain rate tensor. This mode leads to a heat flux in the absence of a temperature gradient and a transport coefficient ξ. In planar Poiseuille flow [12] this heat flux mode introduces a term in the temperature profile that is quadratic in the coordinate, as opposed to the standard temperature profile that is purely quartic in the coordinate [13]. Despite this change in the temperature profile, the heat flux remains unchanged. Todd and co-workers have recently studied planar Poiseuille flow using a sixth-order polynomial fit to the streaming velocity when calculating the pressure tensor [14] and a quadratic fit for the heat flux vector [15]. For the Evans method of calculating the thermal conductivity [6] there has been considerable work done [16] investigating the presence of solitonlike waves of energy (or enthalpy) propagating through the fluid at supersonic speeds. More recently, there have been a number of numerical studies of coupled transport processes in nonequilibrium situations. These methods have been used to calculate the thermal conductivity of a weakly shearing Lennard-Jones fluid [17]. Evans [18] and Daivis and Evans [19] have also calculated the thermal conductivity for strongly shearing fluids subjected to a weak temperature gradient.

In most previous nonequilibrium molecular-dynamics studies the streaming velocity is equal either to zero or to some known functional form (such as the linear streaming velocity profile in planar Couette flow). The STF method and Poiseuille flow are two methods where the streaming velocity contains free parameters (either the amplitude or the functional form). For the STF method the fundamental k vector is only one of the possible disturbances that is consistent with the periodic boundary conditions and indeed any higher harmonic of the sinusoidal force can also be excited. The question that arises is how many harmonics do we consider to be part of the streaming velocity. Clearly all the harmonics cannot be included as that would lead to the whole of each particle's velocity being considered as the streaming velocity and hence there is no thermal component. Making the separation between streaming and thermal motion by choosing a fixed number of harmonics effectively introduces a spatial average. A different class of allowed streaming velocities is associated with a two-dimensional k-vector disturbance and we refer to the first of these as four-roller flow (4RF) [20], so named for the four counterrotating vortices in each simulation cell. In this paper we investigate the k-vector dependence of the transport coefficients for 4RF.

II. MACROSCOPIC HYDRODYNAMICS

Hydrodynamics is based upon a set of exact equations that relate the fluxes of the conserved quantities, namely, mass, momentum, and energy, to various gradients. The derivation we give is appropriate for both two- and three-dimensional systems. The standard conservation equations in Eulerian form are

$$\frac{\partial}{\partial t}\rho(\mathbf{r},t)=-\boldsymbol{\nabla}\cdot[\rho(\mathbf{r},t)\mathbf{u}(\mathbf{r},t)], \tag{1}$$

$$\frac{\partial}{\partial t}[\rho(\mathbf{r},t)\mathbf{u}(\mathbf{r},t)]=\boldsymbol{\nabla}\cdot[\rho(\mathbf{r},t)\mathbf{u}(\mathbf{r},t)\mathbf{u}(\mathbf{r},t)+\underline{\underline{\mathbf{P}}}(\mathbf{r},t)]+\mathbf{F}^{\mathrm{ext}}(\mathbf{r},t), \tag{2}$$

$$\frac{\partial}{\partial t}[\rho(\mathbf{r},t)e(\mathbf{r},t)]=\boldsymbol{\nabla}\cdot[\rho(\mathbf{r},t)e(\mathbf{r},t)\mathbf{u}(\mathbf{r},t)+\mathbf{J}_Q(\mathbf{r},t)+\underline{\underline{\mathbf{P}}}(\mathbf{r},t)\cdot\mathbf{u}(\mathbf{r},t)]+\mathbf{u}(\mathbf{r},t)\cdot\mathbf{F}^{\mathrm{ext}}(\mathbf{r},t), \tag{3}$$

which relate the mass density $\rho(\mathbf{r},t)$, streaming velocity $\mathbf{u}(\mathbf{r},t)$, and energy density $\rho(\mathbf{r},t)e(\mathbf{r},t)$ to the pressure tensor $\underline{\underline{\mathbf{P}}}(\mathbf{r},t)$ and heat flux vector $\mathbf{J}_Q(\mathbf{r},t)$. Here $\mathbf{F}^{\mathrm{ext}}(\mathbf{r},t)$ is an external force density (force per unit volume) that couples to each fluid element.

It is natural to separate the energy density $\rho(\mathbf{r},t)\mathbf{u}(\mathbf{r},t)$ into two distinct terms: a convective energy density $\frac{1}{2}\rho(\mathbf{r},t)\mathbf{u}(\mathbf{r},t)^2$ and an internal energy density $\rho(\mathbf{r},t)U(\mathbf{r},t)$, where

$$\rho(\mathbf{r},t)e(\mathbf{r},t)=\tfrac{1}{2}\rho(\mathbf{r},t)\mathbf{u}(\mathbf{r},t)^2+\rho(\mathbf{r},t)U(\mathbf{r},t). \tag{4}$$

Substituting this equation into Eq. (3) and using the mass and momentum conservation equations and the vector identities $\mathbf{u}\cdot[\boldsymbol{\nabla}\cdot(\rho\mathbf{u}\mathbf{u})]-\boldsymbol{\nabla}\cdot(\rho\mathbf{u}\frac{1}{2}u^2)=\frac{1}{2}u^2\boldsymbol{\nabla}\cdot(\rho\mathbf{u})$ and $\boldsymbol{\nabla}\cdot(\underline{\underline{\mathbf{P}}}\cdot\mathbf{u})=\underline{\underline{\mathbf{P}}}^T:\boldsymbol{\nabla}\mathbf{u}+\mathbf{u}\cdot(\boldsymbol{\nabla}\cdot\underline{\underline{\mathbf{P}}})$ gives the internal energy equation

$$\frac{\partial}{\partial t}[\rho(\mathbf{r},t)U(\mathbf{r},t)]=-\boldsymbol{\nabla}\cdot[\rho(\mathbf{r},t)U(\mathbf{r},t)\mathbf{u}(\mathbf{r},t)+\mathbf{J}_Q(\mathbf{r},t)]-\underline{\underline{\mathbf{P}}}(\mathbf{r},t)^T:\boldsymbol{\nabla}\mathbf{u}(\mathbf{r},t) \tag{5}$$

and the streaming kinetic-energy equation

$$\frac{\partial}{\partial t}[\tfrac{1}{2}\rho(\mathbf{r},t)\mathbf{u}(\mathbf{r},t)^2]=-\boldsymbol{\nabla}\cdot[\tfrac{1}{2}\rho(\mathbf{r},t)\mathbf{u}(\mathbf{r},t)^2\mathbf{u}(\mathbf{r},t)]-\mathbf{u}(\mathbf{r},t)\cdot[\boldsymbol{\nabla}\cdot\underline{\underline{\mathbf{P}}}(\mathbf{r},t)]+\mathbf{u}(\mathbf{r},t)\cdot\mathbf{F}^{\mathrm{ext}}(\mathbf{r},t). \tag{6}$$

Notice that there is no external force density term in the equation for the internal energy. In the macroscopic picture the only effect of an external field is to accelerate fluid elements, increasing the streaming kinetic energy; thus, in removing the streaming components to obtain the internal energy, the direct effect of the external field is removed.

It is more convenient to consider the Fourier transforms of the conserved quantities and to write the conservation equations as a function of $\mathbf{k}$. We define the Fourier transform of an arbitrary real tensorial function $\underline{\underline{\mathbf{T}}}(\mathbf{r})$ to be

$$\underline{\underline{\mathbf{T}}}(\mathbf{k}) = \frac{1}{L^2} \int_0^L dx \int_0^L dy \; \underline{\underline{\mathbf{T}}}(\mathbf{r}) \mathbf{e}^{i\mathbf{k}\cdot\mathbf{r}}. \tag{7}$$

For systems that we will consider, the periodic boundary conditions used in computer simulations imply that there is a discrete spectrum of allowed $\mathbf{k}$ vectors [$\mathbf{k}=(2\pi/L)(n,m)$, where n and m are integers and L is the length of the simulation cell]. The original function $\underline{\underline{\mathbf{T}}}(\mathbf{r})$ can be reconstructed using

$$\underline{\underline{\mathbf{T}}}(\mathbf{r}) = \sum_{\mathbf{k}} \; \underline{\underline{\mathbf{T}}}(\mathbf{k}) e^{-i\mathbf{k}\cdot\mathbf{r}}. \tag{8}$$

If $\underline{\underline{\mathbf{T}}}(\mathbf{r})$ is a real function then the Fourier coefficient $\mathrm{Re}\{\underline{\underline{\mathbf{T}}}(\mathbf{k})\}$ is even in $\mathbf{k}$ and $\mathrm{lm}\{\underline{\underline{\mathbf{T}}}(\mathbf{k})\}$ is odd. Using the definition of the Fourier transform and its inverse, the Kronecker delta and the delta function are given by

$$\delta_{\mathbf{k},\mathbf{k}'} = \frac{1}{L^2} \int d\mathbf{r} \; e^{-i(\mathbf{k}-\mathbf{k}')\cdot\mathbf{r}},$$

$$\delta(\mathbf{r}-\mathbf{r}') = \frac{1}{L^2} \sum_{\mathbf{k}} \; e^{-i\mathbf{k}\cdot(\mathbf{r}-\mathbf{r}')}.$$

In a steady state, in an Eulerian frame each of the hydrodynamic densities lose their explicit time dependence, so the partial time derivatives on the left-hand side (LHS) of Eqs. (1)–(3) are zero. Fourier transforming these equations gives

$$\mathbf{k}\cdot\sum_{\mathbf{k}'} \; \rho(\mathbf{k}-\mathbf{k}')\mathbf{u}(\mathbf{k}') = 0, \tag{9}$$

$$-i\sum_{\mathbf{k}''} \; \sum_{\mathbf{k}'} \; \rho(\mathbf{k}-\mathbf{k}'')\mathbf{u}(\mathbf{k}''-\mathbf{k}')\cdot\mathbf{k}'\mathbf{u}(\mathbf{k}') = i\mathbf{k}\cdot\mathbf{P}(\mathbf{k}) + \mathbf{F}^{\mathrm{ext}}(\mathbf{k}), \tag{10}$$

$$-i\sum_{\mathbf{k}''} \; \sum_{\mathbf{k}'} \; \rho(\mathbf{k}-\mathbf{k}'')\mathbf{u}(\mathbf{k}''-\mathbf{k}')\cdot\mathbf{k}'U(\mathbf{k}') = i\mathbf{k}\cdot\mathbf{J}_Q(\mathbf{k}) + \sum_{\mathbf{k}'} \; \underline{\underline{\mathbf{P}}}(\mathbf{k}')^T : i(\mathbf{k}-\mathbf{k}')\mathbf{u}(\mathbf{k}-\mathbf{k}'). \tag{11}$$

Notice that the discrete convolutions imply a particular coupling between the Fourier coefficients at different $\mathbf{k}$ vectors. These arise from the nonlinear terms in the conservation equations. To close these equations we use the constitutive equations. The constitutive relation for the pressure tensor is

$$\underline{\underline{\mathbf{P}}}(\mathbf{r}) = -2\eta(\underline{\underline{\nabla\mathbf{u}}}^0(\mathbf{r})^s - [\eta_B\nabla\cdot\mathbf{u}(\mathbf{r}) - \rho)\underline{\underline{\mathbf{I}}}, \tag{12}$$

where η is the shear viscosity, η_B is the bulk viscosity, and $\underline{\underline{\mathbf{I}}}$ is the identity matrix. For divergence-free flow the symmetric traceless part of the strain rate tensor reduces to

$$[\underline{\underline{\nabla\mathbf{u}}}^0(\mathbf{r})]^s = \tfrac{1}{2}\{\underline{\underline{\nabla\mathbf{u}}}(\mathbf{r}) + [\underline{\underline{\nabla\mathbf{u}}}(\mathbf{r})]^T\}.$$

The constitutive relation for the heat flux vector is

$$\mathbf{J}_Q(\mathbf{r}) = -\lambda\nabla T(\mathbf{r}) - \xi\nabla\{[\underline{\underline{\nabla\mathbf{u}}}^0(\mathbf{r})]^s : [\underline{\underline{\nabla\mathbf{u}}}^0(\mathbf{r})]^s\}, \tag{13}$$

where λ is the thermal conductivity. These two equations eliminate the pressure tensor and heat flux vector by defining the transport coefficients for viscosity and thermal conductivity. The second term in the constitutive equation for the heat flux vector is that proposed by Baranyai, Evans and Daivis [11] and indicates that a heat current can be generated in the absence of a temperature gradient. This introduces an extra transport coefficient ξ, which is related to the gradient of the square of the strain rate tensor.

Fourier transforming the constitutive equations leads to expressions for the pressure tensor and heat flux where only terms of the same $\mathbf{k}$ vector are coupled by the standard transport coefficients as

$$\underline{\underline{\mathbf{P}}}(\mathbf{k}) = i\eta[\mathbf{k}\mathbf{u}(\mathbf{k}) + \mathbf{u}(\mathbf{k})\mathbf{k}] + p(\mathbf{k})\underline{\underline{\mathbf{I}}}, \tag{14}$$

$$\mathbf{J}_Q(\mathbf{k}) = i\mathbf{k}\lambda T(\mathbf{k}) - i\mathbf{k}\frac{\xi}{2}\sum_{\mathbf{k}'} \; \{[(\mathbf{k}-\mathbf{k}')\cdot\mathbf{u}(\mathbf{k}')] \times [\mathbf{k}'\cdot\mathbf{u}(\mathbf{k}-\mathbf{k}')] + [(\mathbf{k}-\mathbf{k}')\cdot\mathbf{k}'] \times [\mathbf{u}(\mathbf{k}')\cdot\mathbf{u}(\mathbf{k}-\mathbf{k}')]\}. \tag{15}$$

The transport coefficient ξ introduces coupling between different $\mathbf{k}$ vector components of the streaming velocity and the heat flux. This arises from the double contraction of the traceless symmetric velocity gradient tensor. In this paper we consider the transport coefficients as constants and thus an explicit $\mathbf{k}$ dependence is not included. Thus the effective transport coefficient at one value of $\mathbf{k}$ may differ from that at another. A more general constitutive relation could be obtained by allowing η to be $\mathbf{k}$ dependent. This would imply a convolution in the $\mathbf{r}$-space constitutive equation, which then includes nonlocal effects.

III. MICROSCOPIC CONNECTIONS

A. Mass conservation

To make the connection between hydrodynamics and microscopic classical mechanics we need definitions of the conserved densities. In the spirit of Irving and Kirkwood [2] we consider a single phase-space trajectory evolving in time and define the mass density at time t [4]. The definition of the mass density on the macroscopic scale for a fluid element is simply the mass of the element divided by its volume. In the quasimicroscopic picture we imagine that the mass of the element is the number of atoms it contains multiplied by the mass of an atom. However, in the microscopic picture the mass density at point $\mathbf{r}$ is zero if there is no particle at position $\mathbf{r}$ and infinite if there is a particle at $\mathbf{r}$. In this way we write the mass density as

$$\rho(\mathbf{r},t)=\sum_i m_i\delta(\mathbf{r}-\mathbf{r}_i(t)). \tag{16}$$

Integrating this expression over a fluid element would then give the number of atoms times the mass. The LHS is a macroscopic hydrodynamic quantity and the right-hand side (RHS) is its microscopic representation. It is important to realize that this definition is consistent with the Eulerian picture in that position $\mathbf{r}$ is fixed in space and the only time dependence on the RHS is the time dependence of $\mathbf{r}_i(t)$, which arises through the motion of the particles. Substituting this mass density into the LHS of the mass conservation equation (1), using the identity

$$\frac{\partial}{\partial \mathbf{r}_i}\,\delta(\mathbf{r}-\mathbf{r}_i)\equiv-\frac{\partial}{\partial \mathbf{r}}\,\delta(\mathbf{r}-\mathbf{r}_i),$$

and comparing it with the RHS of Eq. (1), we see that the instantaneous momentum density is

$$\rho(\mathbf{r},t)\mathbf{u}(\mathbf{r},t)=\mathbf{J}(\mathbf{r},t)=\sum_i m_i\dot{\mathbf{r}}_i\delta(\mathbf{r}-\mathbf{r}_i). \tag{17}$$

There is no instantaneous representation for the streaming velocity $\mathbf{u}(\mathbf{r},t)$ at the particle level that can be constructed from the instantaneous representations for $\rho(\mathbf{r},t)$ and $\mathbf{J}(\mathbf{r},t)$. Taking the ratio $\mathbf{J}(\mathbf{r},t)/\rho(\mathbf{r},t)$ would give the streaming velocity to be the particle velocity at the position of each particle and undefined elsewhere. This is not a useful definition of the streaming velocity. Any realistic representation for $\mathbf{u}(\mathbf{r},t)$ necessarily involves some form of coarse graining in either space or time. Once a streaming velocity has been determined (by whatever means), we can divide the laboratory velocity of each particle into a thermal part $\mathbf{v}_i$ and a streaming part $\mathbf{u}(\mathbf{r}_i)$, that is,

$$\dot{\mathbf{r}}_i=\mathbf{v}_i+\mathbf{u}(\mathbf{r}_i).$$

Using this representation, we can write the instantaneous momentum density as

$$\mathbf{J}(\mathbf{r},t)=\sum_i m_i\mathbf{v}_i\delta(\mathbf{r}-\mathbf{r}_i)+\rho(\mathbf{r},t)\mathbf{u}(\mathbf{r},t) \tag{18}$$

and we see immediately, from the definition of $\mathbf{J}(\mathbf{r},t)$ in Eq. (17), that the thermal velocities do not contribute to the momentum current as

$$\sum_i m_i\mathbf{v}_i\delta(\mathbf{r}-\mathbf{r}_i)=0. \tag{19}$$

A key step in all the microscopic derivations is that if $f(\mathbf{r})$ is a simple function of $\mathbf{r}$ (which is not an operator), then $f(\mathbf{r})\,\delta(\mathbf{r}-\mathbf{r}_i)\equiv f(\mathbf{r}_i)\,\delta(\mathbf{r}-\mathbf{r}_i)$. There are some subtle points with regard to the interpretation of Eq. (18). Both $\mathbf{J}(\mathbf{r},t)$ and $\rho(\mathbf{r},t)\mathbf{u}(\mathbf{r},t)$ are macroscopic quantities, defined for a fluid element, and are numerically equal. This implies that at the fluid element level Eq. (19) is equal to zero. Clearly this separation between thermal and streaming parts is physically correct. We can also interpret this equation as a condition that the streaming velocity of a fluid element must satisfy. Thus

$$\mathbf{u}(\mathbf{r})=\frac{\sum_{i\in E(\mathbf{r})} m_i\dot{\mathbf{r}}_i\delta(\mathbf{r}-\mathbf{r}_i)}{\sum_{i\in E(\mathbf{r})} m_i\delta(\mathbf{r}-\mathbf{r}_i)}, \tag{20}$$

where the summation is over particles within fluid element $E(\mathbf{r})$, but this form for $\mathbf{u}(\mathbf{r})$ will change discontinuously as particles enter or leave the fluid element. The approach that we will adopt in the formal derivations that follow is to derive the microscopic representations using the full particle velocities and then make the separation into thermal and streaming components.

B. Momentum conservation

Substituting the microscopic representation for the momentum density [Eq. (17)] into the RHS of the momentum conservation equation (2), we find that

$$\frac{\partial}{\partial t}\,[\rho(\mathbf{r},t)\mathbf{u}(\mathbf{r},t)]=-\frac{\partial}{\partial \mathbf{r}}\cdot\sum_i m_i\dot{\mathbf{r}}_i\dot{\mathbf{r}}_i\delta(\mathbf{r}-\mathbf{r}_i)+\sum_i m_i\ddot{\mathbf{r}}_i\delta(\mathbf{r}-\mathbf{r}_i). \tag{21}$$

At this point we use the equations of motion to write $m_i\ddot{\mathbf{r}}_i=\mathbf{F}_i+\mathbf{F}_i^e-\alpha m_i[\dot{\mathbf{r}}_i-\mathbf{u}(\mathbf{r}_i)]$, where $\mathbf{F}_i^e$ denotes the external force on particle i and the last term is the isokinetic thermostat [4]. For the external component of the force alone, consider a small volume element $E(\mathbf{r})$ such that the force exerted on each particle is equal; then

$$\sum_i \mathbf{F}^e(\mathbf{r}_i)\,\delta(\mathbf{r}-\mathbf{r}_i)=\mathbf{F}^e(\mathbf{r},t)\sum_i\,\delta(\mathbf{r}-\mathbf{r}_i)=\mathbf{F}^e(\mathbf{r},t)n(\mathbf{r},t)=\mathbf{F}^{\rm ext}(\mathbf{r},t), \tag{22}$$

where $n(\mathbf{r},t)$ is the number density, $\mathbf{F}^e(\mathbf{r},t)$ is the force on the volume element, and $\mathbf{F}^{\rm ext}(\mathbf{r},t)$ is the force density that appears in macroscopic conservation equations. When the thermostating term is substituted into Eq. (21) it gives zero contribution from Eq. (19) (on the volume element length scale).

In the remainder of this treatment we will assume that the internal forces arise from pairwise interactions (the introduction of three-body forces is possible, but more complicated). For pair interactions

$$\sum_i \mathbf{F}_i\delta(\mathbf{r}-\mathbf{r}_i)=\sum_{i,j}\,\mathbf{F}_{ij}\delta(\mathbf{r}-\mathbf{r}_i)=\tfrac{1}{2}\Big(\sum_{i,j}\,\mathbf{F}_{ij}[\,\delta(\mathbf{r}-\mathbf{r}_i)-\delta(\mathbf{r}-\mathbf{r}_j)]\Big),$$

where $\mathbf{F}_{ij}$ is the force on particle i due to particle j. Treating the δ function as an analytic function, we may expand $\delta(\mathbf{r}-\mathbf{r}_j)$ in a Taylor series about $\delta(\mathbf{r}-\mathbf{r}_i)$. This gives the $O_{ij}[\mathbf{r}]$ operator that can be written either as an operator on functions of $\mathbf{r}$ or as an operator on functions of $\mathbf{r}_i$,

$$\delta(\mathbf{r}-\mathbf{r}_i)-\delta(\mathbf{r}-\mathbf{r}_j)=\frac{\partial}{\partial\mathbf{r}}\cdot\mathbf{r}_{ij}O_{ij}[\mathbf{r}]\delta(\mathbf{r}-\mathbf{r}_i)$$
$$=\frac{\partial}{\partial\mathbf{r}}\cdot\mathbf{r}_{ij}\int_0^1 d\lambda\ \delta(\mathbf{r}-\mathbf{r}_i-\lambda\mathbf{r}_{ij}), \tag{23}$$

where $\mathbf{r}_{ij}=\mathbf{r}_j-\mathbf{r}_i$. The O_{ij} operator is a cumbersome infinite series [15], but the second equality gives a much more useful integral representation [21]. Both of these forms allow us to factor out the derivative with respect to $\mathbf{r}$ that we need to match the hydrodynamic equation (2). The momentum conservation equation then gives

$$\rho(\mathbf{r},t)\mathbf{u}(\mathbf{r},t)\mathbf{u}(\mathbf{r},t)+\underline{\underline{\mathbf{P}}}(\mathbf{r},t)$$
$$=\sum_i\ m_i\dot{\mathbf{r}}_i\dot{\mathbf{r}}_i\delta(\mathbf{r}-\mathbf{r}_i)-\tfrac{1}{2}\sum_i\ \mathbf{r}_{ij}\mathbf{F}_{ij}\int_0^1 d\lambda\,\delta(\mathbf{r}-\mathbf{r}_i-\lambda\mathbf{r}_{ij}).$$

We now divide the velocity of each particle into thermal and streaming parts and we find that the streaming component on the RHS is equal to the streaming term on the LHS, that is, $\rho(\mathbf{r})\mathbf{u}(\mathbf{r})\mathbf{u}(\mathbf{r})$. Therefore, we can identify the microscopic representation for the local pressure tensor at position $\mathbf{r}$ at time t as

$$\underline{\underline{\mathbf{P}}}(\mathbf{r},t)=\sum_i\ m_i\mathbf{v}_i\mathbf{v}_i\delta(\mathbf{r}-\mathbf{r}_i)$$
$$-\tfrac{1}{2}\sum_{i,j}\ \mathbf{r}_{ij}\mathbf{F}_{ij}\int_0^1 d\lambda\,\delta(\mathbf{r}-\mathbf{r}_i-\lambda\mathbf{r}_{ij}). \tag{24}$$

C. Energy conservation

To obtain the microscopic representation for the heat flux vector $\mathbf{J}_Q(\mathbf{r},t)$, we define the instantaneous microscopic energy density to be

$$\rho e(\mathbf{r},t)=\sum_{i=1}^N\ e_i\delta(\mathbf{r}-\mathbf{r}_i(t)), \tag{25}$$

where $e_i=\frac{1}{2}m_i\dot{\mathbf{r}}^2+\frac{1}{2}\Sigma_j\phi(\mathbf{r}_{ij})$ is the energy of particle i. There is an implicit assumption in this definition of the energy density. That is, that for each pair interaction, half the potential interaction energy is assigned to each of the particles. For homogeneous, isotropic systems this assumption seems plausible, but in other circumstances, far from equilibrium, little is known of the validity of this assumption. Substituting the microscopic representation of the energy density into the macroscopic energy conservation equation (3), differentiating the energy of particle i and the δ function with respect to time, combining these two terms, and using the integral representation of the O_{ij} operator, this becomes

$$\rho(\mathbf{r},t)e(\mathbf{r},t)\mathbf{u}(\mathbf{r},t)+\mathbf{J}_Q(\mathbf{r},t)+\underline{\underline{\mathbf{P}}}(\mathbf{r},t)\cdot\mathbf{u}(\mathbf{r},t)$$
$$=\sum_i\ e_i\dot{\mathbf{r}}_i\delta(\mathbf{r}-\mathbf{r}_i)-\tfrac{1}{2}\sum_{i,j}\ \mathbf{r}_{ij}\mathbf{F}_{ij}\cdot\dot{\mathbf{r}}_i$$
$$\times\int_0^1 d\lambda\ \delta(\mathbf{r}-\mathbf{r}_i-\lambda\mathbf{r}_{ij}). \tag{26}$$

The microscopic external field energy *source* term matches that in the macroscopic conservation equation [using Eq. (22)] but the thermostat *sink* term does not (because the thermostating mechanism was not explicitly considered in the macroscopic treatment). We now divide the velocity of each particle into thermal and streaming parts and find that the streaming components on the RHS cancel with the streaming term $\rho(\mathbf{r},t)e(\mathbf{r},t)\mathbf{u}(\mathbf{r},t)$ on the LHS. Using the microscopic form for the pressure tensor obtained previously in Eq. (24), we find that the heat flux vector can be written as

$$\mathbf{J}_Q(\mathbf{r},t)=\sum_i\ \{e_i\mathbf{v}_i-m_i\mathbf{v}_i\mathbf{v}_i\cdot\mathbf{u}(\mathbf{r}_i)\}\delta(\mathbf{r}-\mathbf{r}_i)$$
$$-\tfrac{1}{2}\sum_{i,j}\ \mathbf{r}_{ij}\mathbf{F}_{ij}\cdot[\mathbf{v}_i+\mathbf{u}(\mathbf{r}_i)-\mathbf{u}(\mathbf{r})]$$
$$\times\int_0^1 d\lambda\ \delta(\mathbf{r}-\mathbf{r}_i-\lambda\mathbf{r}_{ij}).$$

However, there are still kinetic streaming components remaining in e_i. Removing these by defining the internal energy of particle i to be $U_i=\frac{1}{2}m_i\mathbf{v}_i^2+\frac{1}{2}\Sigma_j\phi_{ij}$, the final result for the heat flux vector is then

$$\mathbf{J}_Q(\mathbf{r},t)=\sum_i\ U_i\mathbf{v}_i\delta(\mathbf{r}-\mathbf{r}_i)-\tfrac{1}{2}\sum_{i,j}\ \mathbf{r}_{ij}\mathbf{F}_{ij}\cdot[\mathbf{v}_i+\mathbf{u}(\mathbf{r}_i)$$
$$-\mathbf{u}(\mathbf{r})]\int_0^1 d\lambda\ \delta(\mathbf{r}-\mathbf{r}_i-\lambda\mathbf{r}_{ij}). \tag{27}$$

This result is equivalent to but substantially simpler than the infinite series representation obtained previously [15]. As Eqs. (24) and (27) are the exact representations for the local pressure tensor and heat flux vector in an arbitrary geometry, they reduce to method of planes results for Poiseuille flow.

In transforming to $\mathbf{k}$ space it is sufficient to Fourier transform the microscopic representations for the pressure tensor and the heat flux vector. The microscopic representation for the $\mathbf{k}$-dependent pressure tensor in two dimensions is given by

$$\mathbf{P}(\mathbf{k},t)=\frac{1}{L^2}\left(\sum_{i=1}^N\ m_i\mathbf{v}_i\mathbf{v}_ie^{i\mathbf{k}\cdot\mathbf{r}_i}-\tfrac{1}{2}\sum_{i,j}^N\ \mathbf{r}_{ij}\mathbf{F}_{ij}G_{ij}(\mathbf{k})\right), \tag{28}$$

where

$$G_{ij}(\mathbf{k})=\int d\mathbf{r}\ e^{i\mathbf{k}\cdot\mathbf{r}}\int_0^1 d\lambda\ \delta(\mathbf{r}-\mathbf{r}_i-\lambda\mathbf{r}_{ij})$$
$$=\frac{e^{i\mathbf{k}\cdot\mathbf{r}_i}-e^{i\mathbf{k}\cdot\mathbf{r}_i}}{i\mathbf{k}\cdot\mathbf{r}_{ij}}.$$

In the limit as $\mathbf{k}\cdot\mathbf{r}_{ij}\to 0$, $G_{ij}(\mathbf{k})\to e^{i\mathbf{k}\cdot\mathbf{r}_i}$. As the force $\mathbf{F}_{ij}=\mathbf{r}_{ij}\phi'(r_{ij})$, it follows that the pressure tensor is symmetric. Similarly, the **k**-space representation for the heat flux vector is the Fourier transform of the **r**-space representation equation (28). The microscopic form for the heat flux vector is

$$\mathbf{J}_Q(\mathbf{k},t)L^2=\sum_i U_i\mathbf{v}_i e^{i\mathbf{k}\cdot\mathbf{r}_i}-\tfrac{1}{2}\sum_{i,j}\mathbf{r}_{ij}\mathbf{F}_{ij}\cdot\left\{\mathbf{v}_i G_{ij}(\mathbf{k})-\int_0^1 d\lambda\; e^{i\mathbf{k}\cdot(\mathbf{r}_i+\lambda\mathbf{r}_{ij})}[\mathbf{u}(\mathbf{r}_i+\lambda\mathbf{r}_{ij})-\mathbf{u}(\mathbf{r}_i)]\right\}. \tag{29}$$

The heat flux vector depends on the explicit form of the streaming velocity $\mathbf{u}(\mathbf{r})$ and its integral along the $\mathbf{r}_{ij}$ vector. Clearly, if the streaming term is constant, the integral term is zero.

IV. THE ALGORITHM FOR FOUR-ROLLER FLOW

Molecular-dynamics simulations allow the calculation of all the **k**-vector components of the densities and fluxes involved in both the conservation equations or the constitutive equations. This enables a systematic study of the validity of the application of hydrodynamics to small periodic systems and the usefulness of particular constitutive relations. Here we consider the application of the microscopic formulation to a particular two-dimensional flow field, four roller flow. The algorithm for 4RF [20] begins with the usual Newtonian equations of motion, to which is added an external force term $\mathbf{F}^e(\mathbf{r}_i)$. Because this external force does work on the system a thermostating mechanism that removes (heat) energy is included in order to obtain a stationary state. We use a Gaussian thermostat and the equations of motion are

$$m_i\ddot{\mathbf{r}}_i=\mathbf{F}_i+\mathbf{F}^e(\mathbf{r}_i)-\alpha m_i\mathbf{v}_i. \tag{30}$$

For the purposes of this simulation, we use the *operational* definition of the temperature T, defined in terms of thermal velocities $\mathbf{v}_i$ as

$$NkT=\tfrac{1}{2}\sum_i m_i\mathbf{v}_i^2. \tag{31}$$

Using Gauss's principle of least constraint [22] to fix the instantaneous value of T yields the thermostating term in Eq. (30). The value of the multiplier α can be calculated by differentiating Eq. (31) and substituting Eq. (30). This form, however, contains a term involving the time derivative of the local fluid velocity $\dot{\mathbf{u}}(\mathbf{r}_i)$. If we assume that this whole term is zero, that is,

$$\sum_i m\mathbf{v}_i\cdot\dot{\mathbf{u}}(\mathbf{r}_i)=0, \tag{32}$$

then the following value of the thermostating multiplier is obtained:

$$\alpha=\frac{\sum_{i=1}^N \mathbf{v}_i\cdot[\mathbf{F}_i+\mathbf{F}^e(\mathbf{r}_i)]}{\sum_{i=1}^N m_i\mathbf{v}_i^2}. \tag{33}$$

It is important to realize that this is an assumption that leads to an approximate value for α, thus exact temperature conservation is not achieved. However, for the standard planar Couette flow geometry this approximation is equivalent to the assumption that the kinetic component of the shear stress P_{xy}^K is equal to zero. For the same soft-sphere fluid as that considered here, at a reduced strain rate of 1.0, the kinetic component of the shear stress is 5% of the total shear stress, hence we expect this approximation to be reasonable. For a molecular-dynamics simulation using Eq. (31) as the definition of the temperature, regular velocity scaling during the simulation maintains the correct temperature, so the approximation in Eq. (32) leads only to a small drift in the temperature between each velocity scaling.

The simplest two-dimensional nonzero, nonplanar disturbance that is consistent with periodic boundary conditions is 4RF. The microscopic 4RF external field is defined as

$$\mathbf{F}^e(\mathbf{r})=F_1(-\sin(k_1x)\cos(k_1y),\cos(k_1x)\sin(k_1y)), \tag{34}$$

where $k_n=2\pi n/L$ and L is the length of the molecular-dynamics cell (which is assumed to be square). The amplitude of the force F_1 is an input parameter. The expected response to this field is a flow of the same functional form, that is,

$$\mathbf{u}(\mathbf{r})=u_1(-\sin(k_1x)\cos(k_1y),\cos(k_1x)\sin(k_1y)), \tag{35}$$

where the amplitude u_1 is an observable. However, it is also possible that for sufficiently large fields higher harmonics may be generated in the flow pattern. As the microscopic external force $\mathbf{F}^e(\mathbf{r})$ and the streaming velocity $\mathbf{u}(\mathbf{r})$ have the same vector symmetry, the Fourier coefficients are

$$\mathbf{F}^e(\pm k_1,\pm k_1)=\frac{iF_1}{4}(\mp 1,\pm 1) \tag{36}$$

and

$$\mathbf{u}(\pm k_1,\pm k_1)=\frac{iu_1}{4}(\mp 1,\pm 1). \tag{37}$$

The $\pm$ signs in the x components correspond to each other and the $\pm$ signs in the y components correspond to each other separately. The Fourier coefficients of macroscopic force density $\mathbf{F}^{\text{ext}}(\mathbf{r})$ are the same as those in Eq. (36), but with an extra factor of the number density n.

As we have stressed, the most important connection between statistical mechanics and hydrodynamics is the identification of the streaming velocity $\mathbf{u}(\mathbf{r},t)$. In a computer simulation it is easy to calculate the Fourier coefficients $\rho(\mathbf{k},t)$ and $\mathbf{J}(\mathbf{k},t)$ to arbitrary order in **k**. Either $\rho(\mathbf{r},t)$ or $\mathbf{J}(\mathbf{r},t)$ can then be reconstructed. Limiting the largest **k** vector in the reconstruction sets a limit on the minimum length scale over which $\rho(\mathbf{r},t)$ or $\mathbf{J}(\mathbf{r},t)$ can vary, thus effectively

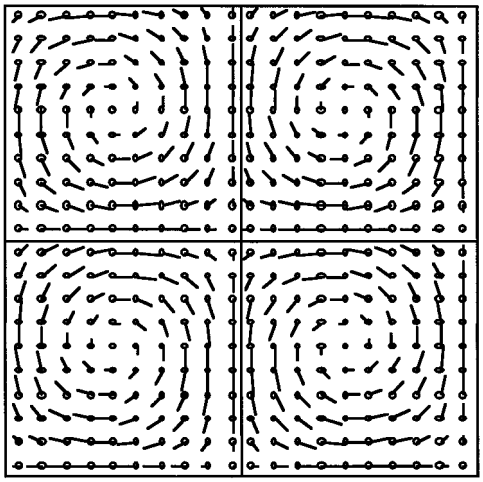

FIG. 1. Vector field velocity profile for 4RF. The flow pattern consists of four counterrotating vortices arranged in a simulation cell.

introducing spatial averaging. Defining $\mathbf{u}(\mathbf{r},t)$ as the ratio of these reconstructed and spatially averaged $\rho(\mathbf{r},t)$ and $\mathbf{J}(\mathbf{r},t)$ gives a well-defined smooth representation for $\mathbf{u}(\mathbf{r},t)$,

$$\mathbf{u}(\mathbf{r},t)=\frac{\sum_{\mathbf{k}}^{k_{\max}}\mathbf{J}(\mathbf{k},t)e^{-i\mathbf{k}\cdot\mathbf{r}}}{\sum_{\mathbf{k}}^{k_{\max}}\rho(\mathbf{k},t)e^{-i\mathbf{k}\cdot\mathbf{r}}}, \tag{38}$$

where $k_{\max}$ is the upper limit of the $\mathbf{k}$-space summation. Any finite truncation of the $\mathbf{k}$-vector sum in the numerator and the denominator introduces a spatial coarse graining and will lead to a smooth representation of $\mathbf{u}(\mathbf{r})$. This could equally well be obtained through temporal coarse graining, though this particular avenue was not examined in this work. The Fourier transform of the field allows free movement to the hydrodynamic description developed previously and is consistent with the periodic boundary conditions. In order to define a hydrodynamic local streaming velocity it is assumed that only the fundamental $\mathbf{k}$ vector of 4RF is excited. This enables the field to generate the position-dependent streaming velocity profile shown in Fig. 1.

V. SIMULATION RESULTS

Molecular-dynamics calculations were performed for two-dimensional systems of 224, 896, 504, and 3584 soft-disk particles of diameter σ [23]. The soft-disk potential $\phi(r)=\varepsilon[(\sigma/r)^{12}-(1/1.5)^{12}]$ for $r<1.5\sigma$ was used with $\phi(r)$ exactly equal to zero for $r>1.5\sigma$. The force calculations were implemented in the program using a cell code routine [24]. The system was fixed at a temperature $kT/\varepsilon=1$ and an average density of $\rho\sigma^2=0.9238$. A fourth-order Gear predictor-corrector algorithm was used to integrate the equations of motion, with a time step in the range $0.002\leqslant\Delta t\leqslant 0.004$. The fundamental k vector is determined by the system size so $k_1=2\pi\sqrt{\rho\sigma^2/N}$, where N is the number of particles. The local streaming velocity was calculated from the Fourier coefficients of the momentum density and mass density each five time steps and that local velocity is then used to separate the random and streaming components of the laboratory velocity of each particle. The results for all density harmonics were calculated for a system with $k_1=0.2018$ and $F_1=0.25$. We refer to this state as our standard state in all that follows. Results were also obtained at other values of k_1 for a range of external field amplitudes F_1. These results illustrate various trends and are presented graphically.

The response of the system to 4RF is measured by calculating the Fourier harmonics for all system properties for $\mathbf{k}=(k_m,k_n)$, where $-4\leqslant m\leqslant 4$ and $-4\leqslant n\leqslant 4$. The simulation results are then substituted in the conservation equations and constitutive relations separately, thus both sides of the conservation equations can be calculated and compared giving a direct test of the applicability of the hydrodynamic description. The constitutive relations are used to obtain values of the transport coefficients for the model fluid, which are effective in the sense that they apply to 4RF at a particular $\mathbf{k}$ value.

A. Mass conservation

The only nonzero responses in the mass density were $\rho(k_2,0)=\rho(0,k_2)=-0.0016$ and $\rho(k_2,k_2)=\rho(k_2,-k_2)=-0.0010$. As these are nearly three orders of magnitude smaller than the mean density, this suggests that the fluid is highly incompressible. At larger values of the external field and for $N=3584$ systems, larger harmonics were generated, although at the most the magnitude of these was only -1%. This is consistent with the incompressibility assumption used frequently in macroscopic hydrodynamics. Here we can use the numerically observed incompressibility to simplify the definition of the streaming velocity in Eq. (38) as the denominator simply reduces to the average density ρ.

B. Momentum conservation

The Fourier coefficients of the streaming velocity have been calculated at our standard state and the results show that the only significant coefficients are those of the fundamental response. All other coefficients were at least two orders of magnitude smaller. As expected, the real parts of the coefficients were zero, but the imaginary parts were nonzero; in particular the 4RF fundamentals give $J_x(k_1,k_1)=J_x(k_1,-k_1)=-J_y(k_1,k_1)=J_y(k_1,-k_1)=-0.211\pm 1$. This confirms the assumption (made previously) that at this value of the external field amplitude $F_1=0.25$ only the fundamental mode of the streaming velocity is excited. Using Eq. (37), we find that $u_1=0.9136$. This, combined with the observed incompressibility, leads to a number of simplifications in the analysis that follows. In particular, the numerator of Eq. (38) in the definition of the streaming velocity is assumed to contain only the fundamental k vectors of 4RF.

Figure 2 shows the relationship between the observed amplitude of the streaming velocity $u_1=4J_y(k_1,k_1)/\rho$ (choosing the y component only because it is positive) and the magnitude of the applied field F_1 at different values of k_1. Apparently there is an approximately linear relationship between the amplitude of the streaming velocity u_1 and the external field F_1 and an increase in u_1 with decreasing k_1.

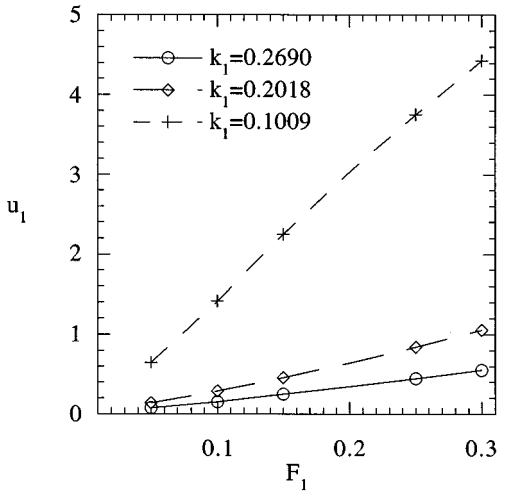

FIG. 2. Graph showing the k vector and external field dependence of the streaming velocity. As the value of k decreases, the physical size of each roller increases, allowing a larger streaming velocity amplitude. The error is smaller than the size of the symbols.

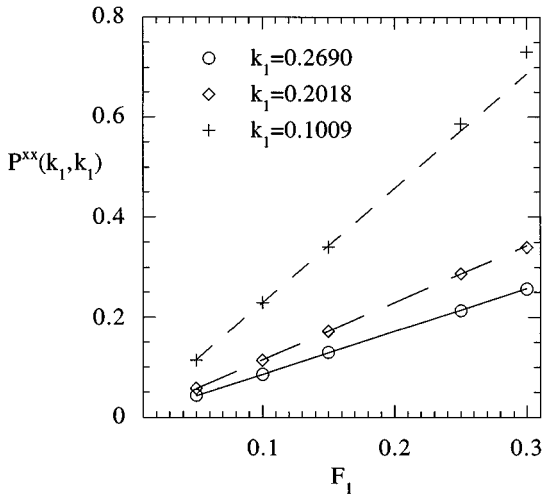

FIG. 3. Graph of the results from the momentum conservation equation for $\mathbf{k}=(k_1,k_1)$ at three different k vectors. The points represent the simulation data accurate to about 2%. The dashed lines are the curves predicted by Eqs. (39) and (40).

1. Case 1: $k=(k_1,\pm k_1)$

As $\mathbf{u}(\mathbf{k})$ is only nonzero for $\mathbf{k}=(\pm k_1,\pm k_1)$, the LHS of Eq. (10) is equal to zero. For the two choices $\mathbf{k}=(k_1,k_1)$ and $\mathbf{k}=(k_1,-k_1)$, the results can be written as

$$P^{xx}(k_1,\pm k_1)\pm P^{yx}(k_1,\pm k_1)=\frac{nF_1}{4k_1}, \tag{39}$$

$$P^{yx}(k_1,\pm k_1)\pm P^{yy}(k_1,\pm k_1)=\mp\frac{nF_1}{4k_1}. \tag{40}$$

Using the fact that the microscopic pressure tensor [Eq. (24)] is symmetric gives

$$P^{xx}(k_1,\pm k_1)-P^{yy}(k_1,\pm k_1)=\frac{nF_1}{2k_1}. \tag{41}$$

The numerical results for our standard state are in excellent agreement with Eqs. (39)–(41). Further, the numerical results strongly suggest that $P^{xy}(\mathbf{k})=P^{yx}(\mathbf{k})=0$ for all values of $\mathbf{k}$ and that therefore $P^{xx}(k_1,\pm k_1)=-P^{yy}(k_1,\pm k_1)=nF_1/4k_1$. For $\mathbf{k}=(k_1,k_1)$, $P^{xx}=0.286$ and $P^{yy}=-0.283$, which gives the LHS equal to 0.569, while the RHS is equal to 0.572. The same result also follows if we assume mechanical stability on the length scale L, so that $P^{xx}(k_1,k_1)+P^{yy}(k_1,k_1)=0$.

In Figure 3 we present the results for $P^{xx}(k_1,k_1)$ as a function of external force amplitude F_1 for various values of k_1. The lines are the predictions from Eqs. (39) and (40).

2. Case 2: $k=(k_2,\pm k_2)$

The LHS of Eq. (10) is equal to zero and there is no external field term, so this gives

$$P^{xx}(k_2,\pm k_2)\pm P^{yx}(k_2,\pm k_2)=0, \tag{42}$$

$$P^{yx}(k_2,\pm k_2)\pm P^{yy}(k_2,\pm k_2)=0. \tag{43}$$

The numerical results agree with these equations, but they also suggest that each individual term is equal to zero.

3. Case 3: $k=(k_2,0)$ and $k=(0,k_2)$

For these k vectors the LHS of Eq. (10) has terms that are nonzero, but there is no external field term. Therefore, it can be shown that

$$P^{xx}(k_2,0)=P^{yy}(0,k_2)=\frac{\rho u_1^2}{8}, \tag{44}$$

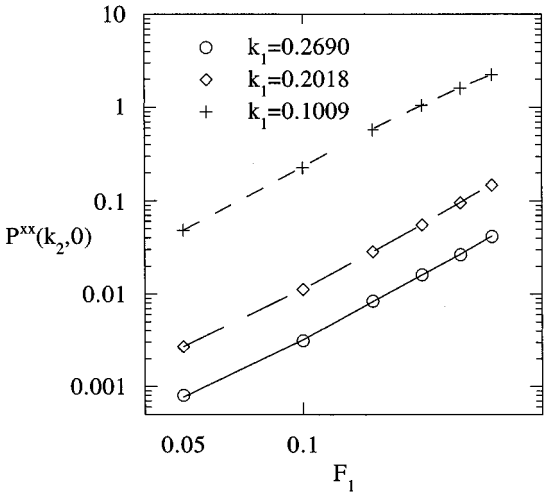

FIG. 4. Graph of the momentum conservation results for $\mathbf{k}=(k_2,0)$. From the symmetry of the system these results are identical to those for $\mathbf{k}=(0,k_2)$. Results for three different k vectors are presented. The points are the simulation values. The dashed lines are the curves predicted by Eq. (44). The error in the simulation values was less than 2%.

TABLE I. Fourier harmonics of the pressure tensor, heat flux vector, and internal energy that are required for the energy conservation energy at the particular values of **k** considered.

k	J_{Qx}	J_{Qy}	**k**	P^{xx}	P^{yy}	U
(k_2,k_2)	$0.0259i$	$0.0294i$	(k_1,k_3)	-0.0223	-0.0020	-0.0041
$(k_2,-k_2)$	$0.0154i$	$-0.0425i$	(k_3,k_1)	0.0020	0.0204	0.0032
			$(k_1,-k_3)$	-0.0218	-0.0015	-0.0028
k	U		$(k_3,-k_1)$	0.0024	0.0216	0.0032
(k_1,k_1)	-0.0009		(k_3,k_3)	-0.0002	0.0000	
$(k_1,-k_1)$	0.0000		$(k_3,-k_3)$	-0.0007	-0.0003	

$$P^{xy}(k_2,0)=P^{yx}(0,k_2)=0. \tag{45}$$

The numerical results for our standard state are in excellent agreement with Eqs. (44) and (45) as $P^{xx}(k_2,0)=0.0950$, $P^{yy}(0,k_2)=0.0950$, and the RHS is equal to 0.0964. Figure 4 compares the numerical results for $P^{xx}(k_2,0)$ as a function of external field amplitude F_1 with the predictions of Eq. (44) at different values of k_1. The agreement is good, except at larger-**k** values.

C. Energy conservation

The energy conservation equation can be thought of as a balance between internal energy *storage* terms, viscous heating *energy production* terms, and the resulting heat current. From the energy conservation equation (11) and, as before, using the numerically observed incompressibility and including only the 4RF fundamentals for the external field and streaming velocity, it can be shown that

$$\begin{aligned}
&\frac{\rho u_1}{4}(1,1)\cdot\{[\mathbf{k}+(k_1,-k_1)]U[\mathbf{k}+(k_1,-k_1)]-[\mathbf{k}-(k_1,-k_1)]\\
&\quad\times U[\mathbf{k}-(k_1,-k_1)]\}+\frac{\rho u_1}{4}(1,-1)\cdot\{[\mathbf{k}+(k_1,k_1)]U[\mathbf{k}+(k_1,k_1)]-[\mathbf{k}-(k_1,k_1)]U[\mathbf{k}-(k_1,k_1)]\}\\
&=i\mathbf{k}\cdot\mathbf{J}_Q(\mathbf{k})+\frac{u_1k_1}{4}\{P^{xx}[\mathbf{k}-(k_1,k_1)]-P^{yy}[\mathbf{k}-(k_1,k_1)]+P^{xx}[\mathbf{k}-(k_1,-k_1)]-P^{yy}[\mathbf{k}-(k_1,-k_1)]\}\\
&\quad+\frac{u_1k_1}{4}\{P^{xx}[\mathbf{k}+(k_1,-k_1)]-P^{yy}[\mathbf{k}+(k_1,-k_1)]+P^{xx}[\mathbf{k}+(k_1,k_1)]-P^{yy}[\mathbf{k}+(k_1,k_1)]\}.
\end{aligned} \tag{46}$$

In obtaining this equation we have assumed that the off-diagonal terms in the pressure tensor $P^{xy}(\mathbf{k})$ and $P^{yx}(\mathbf{k})$ are zero. We now consider different choices for **k**.

1. Case 1: $\mathbf{k}=(k_1,\pm k_1)$

For this value of **k**, due to the symmetry of the system we expect that $P^{xx}(0,0)=P^{yy}(0,0)$ and from Eqs. (42) and (43) that $\underline{\underline{\mathbf{P}}}(k_2,k_2)=0$, so Eq. (46) reduces to

$$\begin{aligned}
&\frac{\rho u_1k_2}{4}\{U(k_2,0)-U(0,\pm k_2)\}\\
&=i(k_1,\pm k_1)\cdot\mathbf{J}_Q(k_1,\pm k_1)+\frac{u_1k_1}{4}\{P^{xx}(k_2,0)\\
&\quad-P^{yy}(k_2,0)+P^{xx}(0,\pm k_2)-P^{yy}(0,\pm k_2)\}.
\end{aligned} \tag{47}$$

For $\mathbf{k}=(k_1,k_1)$, the simulation results (Table I) for the Fourier coefficients on the LHS give $U(k_2,0)-U(0,k_2)=0.0384-0.0393=-0.0009$ and the last term of the RHS gives $P^{xx}(k_2,0)-P^{yy}(k_2,0)+P^{xx}(0,k_2)-P^{yy}(0,k_2)=(0.0841-0.0950+0.0950-0.0844)=-0.0003$. The numerical results for our standard state suggest that each of these terms is individually equal to zero. On symmetry grounds the LHS of Eq. (46) can be expected to be zero. This leaves the heat flux vector terms as the only nonzero contributions, so

$$(k_1,\pm k_1)\cdot[J_{Qx}(k_1,\pm k_1)\pm J_{Qy}(k_1,\pm k_1)]=0. \tag{48}$$

The standard state gives $\mathbf{J}_Q(k_1,k_1)=(0.0346,-0.0340)i$ and $\mathbf{J}_Q(k_1,-k_1)=(0.0369,0.0371)i$, both of which satisfy Eq. (48) almost exactly.

2. Case 2: $\mathbf{k}=(k_2,\pm k_2)$

In this case, combining Eq. (41) with Eq. (46) gives

$$\frac{\rho u_1}{4}(k_1+k_3)\{U(k_3,\pm k_1)-U(k_1,\pm k_3)\}$$
$$=i(k_2,\pm k_2)\cdot\mathbf{J}_Q(k_2,\pm k_2)+\frac{nu_1F_1}{8}$$
$$+\frac{u_1k_1}{4}\{P^{xx}(k_1,\pm k_3)-P^{yy}(k_1,\pm k_3)$$
$$+P^{xx}(k_3,\pm k_1)-P^{yy}(k_3,\pm k_1)\}$$
$$+\frac{u_1k_1}{4}\{P^{xx}(k_3,\pm k_3)-P^{yy}(k_3,\pm k_3)\}. \quad (49)$$

For our standard state the responses in many of the terms in Eq. (49) are small, but probably not negligible.

For $\mathbf{k}=(k_2,k_2)$, including the numerical results for all terms in Eq. (49), the standard state gives the LHS equal to 0.0012 and the RHS equal to 0.0023. For $\mathbf{k}=(k_2,-k_2)$, the LHS is equal to 0.0010 and the RHS is equal to 0.0012. This agreement is impressively good. If, however, we ignore all higher harmonics in Eq. (49), then

$$(k_2,\pm k_2)\cdot\mathbf{J}_Q(k_2,\pm k_2)=-\frac{nu_1F_1}{8}; \quad (50)$$

for our standard state at $\mathbf{k}=(k_2,k_2)$ this gives the LHS equal to 0.0223 and at $\mathbf{k}=(k_2,-k_2)$ this gives the LHS equal to 0.0234, while for both of these the RHS is equal to 0.0264. Clearly, including the higher harmonics in both the internal energy and the pressure reduces the discrepancy between the LHS and the RHS at $\mathbf{k}=(k_2,k_2)$, from 0.0041 to 0.0011, and for $\mathbf{k}=(k_2,-k_2)$, from 0.0030 to 0.0002.

3. Case 3: $\mathbf{k}=(k_2,0)$ and $\mathbf{k}=(0,k_2)$

For these two values of $\mathbf{k}$, Eq. (46), using Eq. (41), gives

$$\frac{\rho u_1}{4}\{-2k_1[U(k_1,k_1)+U(k_1,-k_1)]$$
$$+(k_3-k_1)[U(k_3,k_1)+U(k_3,-k_1)]\}$$
$$=i(k_2,0)\cdot\mathbf{J}_Q(k_2,0)+\frac{nu_1F_1}{4}+\frac{u_1k_1}{4}\{P^{xx}(k_3,k_1)$$
$$-P^{yy}(k_3,k_1)+P^{xx}(k_3,-k_1)-P^{yy}(k_3,-k_1)\} \quad (51)$$

and

$$\frac{\rho u_1}{4}\{2k_1[U(k_1,k_1)+U(k_1,-k_1)]+(k_1-k_3)[U(k_1,k_3)$$
$$+U(k_1,-k_3)]\}$$
$$=i(0,k_2)\cdot\mathbf{J}_Q(0,k_2)+\frac{nu_1F_1}{4}+\frac{u_1k_1}{4}\{P^{xx}(k_1,k_3)$$
$$-P^{yy}(k_1,k_3)+P^{xx}(k_1,-k_3)-P^{yy}(k_1,-k_3)\}. \quad (52)$$

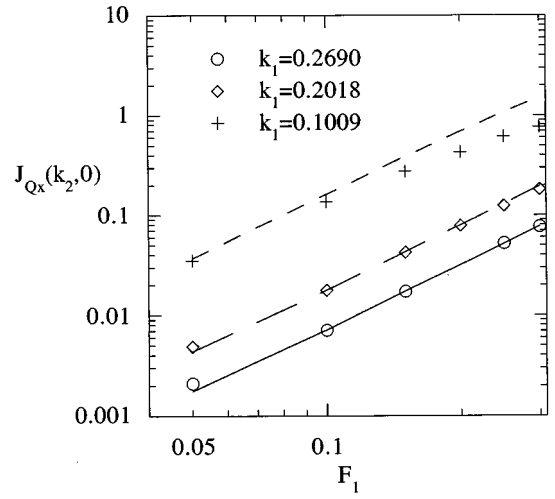

FIG. 5. Graph of the internal energy conservation for $\mathbf{J}_{Qx}(k_2,0)$. Results for the three different k vectors are shown. The points are the values obtained from the simulation. A logarithmic scale is used on the y axis for ease of presentation. The agreement for larger values of k was within statistical error, although a significant deviation occurred for $k_1=0.1009$.

If we assume that the LHSs of Eqs. (51) and (52) are both zero, as the coefficients $U(k_1,\pm k_1)\approx 0$, and on the RHS of each equation the coefficients $P^{xx}(k_1,\pm k_3)=P^{yy}(k_1,\pm k_3)=P^{xx}(k_3,\pm k_1)=P^{yy}(k_3,\pm k_1)\approx 0$, then we obtain the simple result that

$$J_{Qx}(k_2,0)=J_{Qy}(0,k_2)=\frac{inu_1F_1}{8k_1}. \quad (53)$$

For our standard state the numerical results give $J_{Qx}(k_2,0)=0.1241i$ and $J_{Qy}(0,k_2)=0.1234i$, while the RHS is equal to $0.1307i$. Taking into account the observed numerical values of all the Fourier coefficients in Eq. (51) gives $J_{Qx}(k_2,0)=0.1250i$ and Eq. (52) gives $J_{Qy}(0,k_2)=0.1275i$. Both of these more careful calculations improve the agreement.

The balance equation (53) for the $\mathbf{k}=(2k_1,0)$ gave good results at higher values of k_1 and lower values of the external field F_1. However, the appearance of higher-order responses led to more significant inconsistencies than those observed for momentum conservation. This suggests that heat transfer is more complicated at larger fields or streaming velocity amplitudes. There are also significant higher harmonics in the heat flux vector, such as $J_{Qx}(k_1,k_3)=-0.0445i$ and $J_{Qy}(k_3,k_1)=0.0398i$. For the standard state at (k_1,k_3), the conservation equation (46) is again accurately satisfied, but at the same state point with $k_1=0.1009$ the conservation equation is not satisfied. Like the discrepancy in $J_{Qx}(k_2,0)$ in Fig. 5 at the same value of k_1, we believe this is due to the neglect of higher harmonics in the streaming velocity, particularly at (k_1,k_3) and (k_3,k_1).

VI. SHEAR VISCOSITY

A. Case 1: $\mathbf{k}=(k_1,\pm k_1)$

From the constitutive relation for the shear viscosity equation (14), it can be shown that $\mathbf{k}$ must be one of the fundamentals for 4RF and that, for example, for $\mathbf{k}=(k_1,k_1)$,

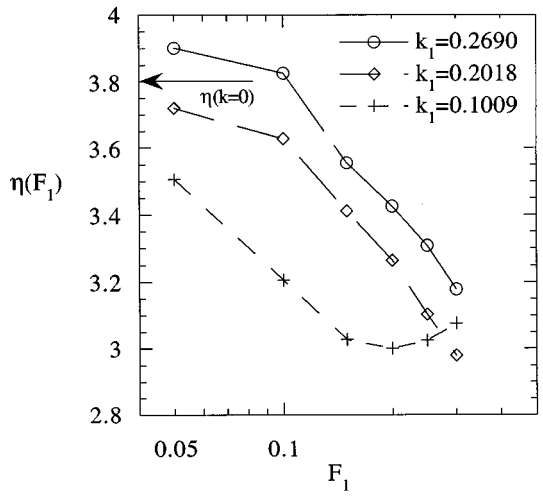

FIG. 6. **k**-dependent shear viscosities for 4RF. As the system size increases, the viscosity decreases, indicating that the greater the number of particles in each roller, the less granular the system.

$$\underline{\underline{\mathbf{P}}}(k_1,k_1)-p(k_1,k_1)\underline{\underline{\mathbf{I}}}=\frac{\eta u_1 k_1}{2}\begin{pmatrix}1 & 0\\ 0 & -1\end{pmatrix}. \tag{54}$$

Combining the two nonzero components gives

$$P^{xx}(k_1,k_1)-P^{yy}(k_1,k_1)=\eta u_1 k_1. \tag{55}$$

Using the result obtained from momentum conservation, Eq. (41), it can be shown that the viscosity is

$$\eta=\frac{nF_1}{2u_1k_1^2}. \tag{56}$$

This route to the shear viscosity and for our standard state this gives the effective viscosity (at $F_1=0.25$) to be 3.1053.

B. Case 2: $\mathbf{k}=(k_2,\pm k_2)$

This is not one of the fundamentals for 4RF so

$$\underline{\underline{\mathbf{P}}}(k_2,\pm k_2)-p(k_2,\pm k_2)\underline{\underline{\mathbf{I}}}=\begin{pmatrix}0 & 0\\ 0 & 0\end{pmatrix}. \tag{57}$$

C. Case 3: $\mathbf{k}=(k_2,0)$ and $\mathbf{k}=(0,k_2)$

Again, this not one of the 4RF fundamentals, so

$$\underline{\underline{\mathbf{P}}}(k_2,0)-p(k_2,0)\underline{\underline{\mathbf{I}}}=\begin{pmatrix}0 & 0\\ 0 & 0\end{pmatrix}. \tag{58}$$

These two cases suggest that the off-diagonal elements of the pressure tensor are zero for these harmonics.

Figure 6 is a graph showing the variation of the viscosity with the applied external field for different values of k_1. The viscosity cannot be accurately determined when the external force is less than ~ 0.1 because the signal-to-noise ratio is too small. Similarly, when the external force becomes too large ($F_1 > \sim 0.3$), higher harmonics of the streaming velocity appear and the thermostating mechanism loses stability. As can be seen from Fig. 6, the viscosity decreases with decreasing k_1. This is expected as k_1 is directly linked to the number of particles and hence the size of the simulation cell L. The larger L, the less granular the roller becomes and the lower the viscosity.

The temperature of the system was fixed by the thermostat term included explicitly in the equations of motion. If the system achieves a steady state, then the average total internal energy $\langle U\rangle=\langle\Sigma_i U_i\rangle$ will attain a steady value. Thus the energy flow into the system from the external field is on average equal to the energy removed by the thermostat. Therefore, the time derivative of $\langle U\rangle$ will be equal to zero. Using the assumption at Eq. (32), this gives

$$2NkT\langle\alpha\rangle=\left\langle\sum_i \mathbf{v}_i\cdot\mathbf{F}^e(\mathbf{r}_i)\right\rangle-\left\langle\sum_i \mathbf{u}(\mathbf{r}_i)\cdot\mathbf{F}_i\right\rangle. \tag{59}$$

If all the particles have the same mass, then using Eq. (8) it can be shown that

$$\begin{aligned}\left\langle\sum_i \mathbf{v}_i\cdot\mathbf{F}^e(\mathbf{r}_i)\right\rangle&=\frac{iF_1}{2m}[(1,-1)\cdot\mathbf{J}(k_1,k_1)\\ &\quad+(1,1)\cdot\mathbf{J}(k_1,-k_1)]\\ &=\frac{nu_1F_1L^2}{2}.\end{aligned}$$

Using the constitutive equation (56), we obtain a second independent route to the shear viscosity

$$\eta=\frac{\rho}{u_1^2k_1^2}\left\{2nkT\langle\alpha\rangle+\frac{1}{N}\left\langle\sum_i \mathbf{u}(\mathbf{r}_i)\cdot\mathbf{F}_i\right\rangle\right\}. \tag{60}$$

For our standard state we can compare values obtained from the two routes to the viscosity. The term $\langle\mathbf{u}(\mathbf{r}_i)\cdot\mathbf{F}_i\rangle = 0.004\,31$ and $\langle\alpha\rangle=0.054\,91$. Thus the viscosity from this route is $\eta=3.1034$, compared with $\eta=3.1053$ from the constitutive equation (56). Such good agreement between the values of the viscosity from the two routes gives us confidence that the thermostating mechanism is working correctly. Equation (59) is simply a balance between the energy supplied to the system by the external field and the energy removed by the thermostat. Although each estimate of the viscosity is not accurate to the number of digits quoted (but rather has an accuracy of about 3–4 %), the difference between the two numbers suggests that almost all the energy is removed by the thermostat (and not by *ad hoc* velocity rescaling). Thus, despite the approximation used to calculate the instantaneous value of α, Eq. (32), the thermostat is working remarkably well.

VII. THERMAL CONDUCTIVITY

The same process can be repeated for the heat flux constitutive equation (15). Direct calculation of the heat flux vector, temperature gradient, and streaming velocity amplitude allows the evaluation of the thermal transport coefficients.

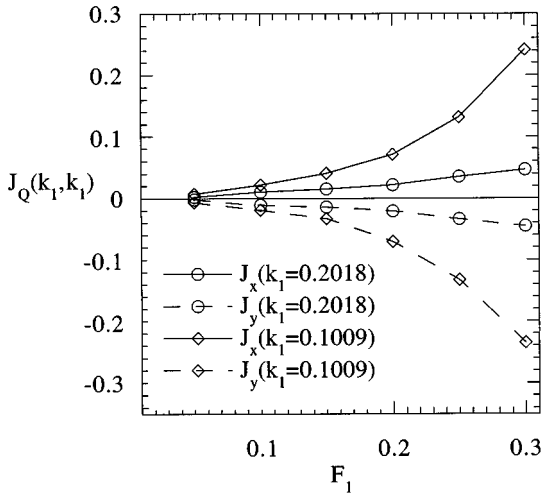

FIG. 7. Plot showing the variation in the (k_1,k_1) harmonic of the heat flux vector. The lines are a linear interpolation between the data points.

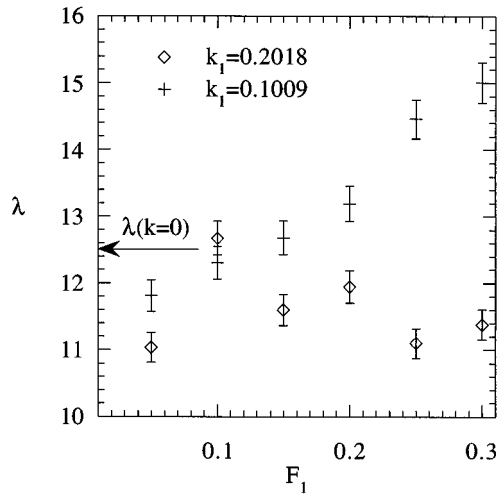

FIG. 8. Thermal conductivities for systems at different k vectors calculated from Eq. (64). The arrow represents the zero-wave-vector limit for the thermal conductivity, calculated by Hansen and Evans [16].

A. Case 1: $\mathbf{k}=(k_1,\pm k_1)$

For this case

$$\mathbf{J}_Q(k_1,\pm k_1)=i(k_1,\pm k_1)\lambda T(k_1,\pm k_1). \tag{61}$$

The numerical results for the standard state give a temperature harmonic of $T(k_1,\pm k_1)=\pm 0.001$. The heat flux vector $\mathbf{J}_Q(k_1,k_1)=(0.0346,-0.0340)i$ and $\mathbf{J}_Q(k_1,-k_1)=(0.0369,0.0371)i$, but the RHS of Eq. (61) would suggest that $|\mathbf{J}_Q|\approx 0.0002$. It is somewhat surprising that there is a response in the heat flux vector at $\mathbf{k}=(k_1,k_1)$ as almost no temperature gradient is observed. Physically, this corresponds to a heat flux in the opposite direction to the streaming velocity. Figure 7 shows the variation of the $\mathbf{J}_Q(k_1,k_1)$ harmonics as a function of field. The lines on the graph are second-order polynomial fits to the numerical data.

B. Case 2: $\mathbf{k}=(k_2,\pm k_2)$

For this case both terms on the RHS of Eq. (15) contribute nonzero terms as

$$\mathbf{J}_Q(k_2,\pm k_2)=i(k_2,\pm k_2)\left(\lambda T(k_2,\pm k_2)+\frac{\xi u_1^2 k_1^2}{8}\right). \tag{62}$$

The numerical results for the standard state are that $\mathbf{J}_Q(k_2,k_2)=(0.0259,0.0294)i$ and $\mathbf{J}_Q(k_2,-k_2)=(0.0154,-0.0425)i$ for a temperature harmonic of $T(k_2,\pm k_2)=0.0067$. From Eq. (62) we can obtain four different equations, each of which has the same RHS. In the four cases the numerical value of the LHS is 9.45, 10.7, 5.7, or 15.7. Taking the average of the LHS, we obtain

$$\lambda+0.624\xi=10.7. \tag{63}$$

This is essentially one equation for the two unknowns λ and ξ.

C. Case 3: $\mathbf{k}=(k_2,0)$ and $\mathbf{k}=(0,k_2)$

This case is also of interest as the second term on the RHS of Eq. (15) is again nonzero. So

$$\mathbf{J}_Q(k_2,0)=i(k_2,0)\left(\lambda T(k_2,0)+\frac{\xi k_1^2 u_1^2}{4}\right) \tag{64}$$

and

$$\mathbf{J}_Q(0,k_2)=i(0,k_2)\left(\lambda T(0,k_2)+\frac{\xi k_1^2 u_1^2}{4}\right). \tag{65}$$

For the standard state $J_{Qx}(k_2,0)=0.1241i$ and $J_{Qx}(0,k_2)=0.1234i$ and the temperature harmonics are $T(k_2,0)=0.0266$ and $T(0,k_2)=0.0277$. This gives a second independent equation involving λ and ξ, that is,

$$\lambda+0.31\xi=11.3. \tag{66}$$

Combining these two equations, we get the following estimates for the two transport coefficients $\lambda=11.9$ and $\xi=-1.9$. The only other numerical estimate for ξ is a very recent result obtained by Todd and Evans [13] for Poiseuille flow, which gives $\xi\approx 70$. The result obtained here is for 4RF geometry and a particular k vector, and external field strength, so a meaningful comparison of these two results is not possible.

The thermal conductivity λ can also be calculated in a more usual nonequilibrium way. That is, we can plot $\lambda+\xi k_1^2 u_1^2/4T(0,k_2)$ as a function of the external field amplitude F_1. As F_1 approaches zero, the second term becomes negligible and we recover the thermal conductivity. Figure 8 shows a plot of the thermal conductivity as a function of the external field amplitude. Hansen and Evans [16] calculate the $\mathbf{k}\to 0$ value of the thermal conductivity for the same system to be of the order of 12.5 ± 0.6. The results obtained here both from Eqs. (63) and (66) and from Fig. 8 are consistent with the value obtained by Hansen and Evans. The nonlinear effects appear to increase with decreasing k_1.

VIII. CONCLUSION

The numerical results for the conservation equations show that the hydrodynamic description of a fluid of 896 particles in periodic boundary conditions is completely consistent with the molecular-dynamics results. In all cases the predictions of the conservation equations agreed with the simulation results. This tests the applicability of hydrodynamics to small systems and verifies the microscopic representations for the pressure tensor and heat flux vector for a system with a nontrivial streaming velocity. The numerical results for the constitutive equations for particular values of the k vector give the effective values of the transport coefficients, but in other cases, such as the nonfundamental k vectors for shear viscosity, they predict the absence of particular harmonic responses. Often in these cases, these are limitations of the constitutive equation as the numerical result show the existence of a nonzero response.

The value of the viscosity at nonzero k vector is not much different from the zero-k-vector result of $\eta=3.80$. As this method is specific to the particular flow pattern and yields results for a discrete set of k vectors, a much more detailed study would be necessary to thoroughly explore the k dependence of the viscosity. The combined use of the constitutive equation for the heat flux, at two different k vectors, allows independent estimates of both the usual thermal conductivity and also the transport coefficient ξ. Our results suggest that for 4RF the thermal conductivity is about $\lambda=11.9$ and the coefficient $\xi\cong-2$. The accuracy of the thermal conductivity is probably better than 10%, with the largest source of error being the extrapolation to zero k. However, for ξ the error bars would be much larger, possibly as much as 100%, even casting doubt on the sign of this term.

The observation of a heat flux component of the same vector character as the streaming velocity but in the opposite direction is somewhat surprising. The are a number of possible reasons for this and further work would be required to determine the physical origin of this effect. There are a number of possible causes. The thermostating mechanism used in this work contains an approximation [Eq. (19)] and although the error associated with that approximation seems small (at most 5% error in the value of α), it may be large enough to account for the extra heat flux ($\sim$0.03). Alternatively, the extra heat flux may be associated with small perturbations of the streaming velocity that were ignored by considering the streaming velocity to have the same functional form as the driving force. If this is the case, then adding higher-order terms to the streaming velocity may remove the effect. Also, it has been noted that the nonlinear hydrodynamic instability associated with the nonequilibrium thermal conductivity algorithm is the appearance of a solitonlike shock wave traveling at supersonic speed whose normal is parallel the applied field [25]. It is certainly possible that a similar nonlinear instability could perturb the streaming velocity and produce an extra heat flux contribution.

ACKNOWLEDGMENTS

We thank the Research School of chemistry, The Australian National University, for support during the course of this work. G.P.M. would particularly like to thank Peter Daivis for valuable discussions.

[1] W. D. McComb, *The Physics of Fluid Turbulence* (Clarendon, Oxford, 1990); D. J. Tritton, *Physical Fluid Dynamics* (Van Nostrand Reinhold, Wokingham, 1985).
[2] J. H. Irving and J. G. Kirkwood, J. Chem. Phys. **18**, 817 (1950).
[3] M. S. Green, J. Chem. Phys. **22**, 398 (1954); R. Kubo, J. Phys. Soc. Jpn. **12**, 570 (1957).
[4] D. J. Evans and G. P. Morriss, *Statistical Mechanics of Nonequilibrium Liquids* (Academic, London, 1990).
[5] W. G. Hoover and W. T. Ashurst, in *Theoretical Chemistry: Advances and Perspectives*, edited by H. Eyring and D. Henderson (Academic, New York, 1975), Vol. 1, p. 1.
[6] D. J. Evans, Phys. Lett. **91A**, 457 (1982).
[7] M. J. Gillan and M. Dixon, J. Phys. C **16**, 869 (1983).
[8] E. M. Gosling, I. R. McDonald, and K. Singer, Mol. Phys. **26**, 1475 (1973).
[9] D. J. Evans, Mol. Phys. **47**, 1165 (1982).
[10] D. J. Evans and R. M. Lynden-Bell, Phys. Rev. A **38**, 5249 (1988); R. K. Standish and D. J. Evans, *ibid.* **41**, 4501 (1990); Phys. Rev. E **48**, 3478 (1993).
[11] A. Baranyai, D. J. Evans, and P. J. Daivis, Phys. Rev. A **46**, 7593 (1992).
[12] S. Y. Liem, D. Brown, and J. H. R. Clarke, Phys. Rev. A **45**, 3706 (1992).
[13] B. D. Todd and D. J. Evans, J. Chem. Phys. **103**, 9804 (1995); B. D. Todd and D. J. Evans, Phys. Rev. E **55**, 2800 (1997).
[14] B. D. Todd, D. J. Evans, and P. J. Daivis, Phys. Rev. E **52**, 1627 (1995).
[15] B. D. Todd, P. J. Daivis, and D. J. Evans, Phys. Rev. E **51**, 4362 (1995).
[16] D. P. Hansen and D. J. Evans, Mol. Phys. **81**, 767 (1993); Mol. Simul. **14**, 409 (1995).
[17] D. J. Evans, Phys. Rev. A **34**, 1449 (1986).
[18] D. J. Evans, Phys. Rev. A **44**, 3630 (1991).
[19] P. J. Daivis and D. J. Evans, Phys. Rev. E **48**, 1058 (1993).
[20] D. R. J. Monaghan, G. P. Morriss, and D. J. Evans, Mol. Phys. **85**, 1151 (1995).
[21] W. Noll, J. Rational Mech. Anal. **4**, 627 (1955).
[22] K. F. Gauss, J. Reine Angew. Math. **IV**, 232 (1829).
[23] W. G. Hoover, M. Ross, K. W. Johnson, D. Henderson, J. A. Barker, and B. C. Brown, J. Chem. Phys. **52**, 4931 (1970).
[24] D. J. Evans and G. P. Morriss, Comput. Phys. Rep. **1**, 297 (1984); M. P. Allen and D. J. Tildesley, *Computer Simulation of Liquids* (Oxford University Press, Oxford, 1987).
[25] D. J. Evans and H. J. M. Hanley, Mol. Phys. **68**, 97 (1989); M. Mareschal and A. Amellal, Phys. Rev. A **37**, 2189 (1988); W. Loose, *ibid.* **40**, 2625 (1989).